Nonlinear Synchronization Control for Short-Range Mobile Sensors Drifting in Geophysical Flows

Cong Wei, Herbert G. Tanner, and M. Ani Hsieh

Abstract— **This paper presents a synchronization controller for mobile sensors that are minimally actuated and can only communicate with each other over a very short range. This work is motivated by ocean monitoring applications where large-scale sensor networks consisting of drifters with minimal actuation capabilities, *i.e.*, *active* drifters, are employed. We assume drifters are tasked to monitor regions consisting of gyre flows where their trajectories are periodic. As drifters in neighboring regions move into each other's proximity, it presents an opportunity for data exchange and synchronization to ensure future rendezvous. We present a nonlinear synchronization control strategy to ensure that drifters will periodically rendezvous and maximize the time they are in their rendezvous regions. Numerical simulations and small-scale experiments validate the efficacy of the control strategy and hint at extensions to large-scale mobile sensor networks.**

I. Introduction

This paper addresses the problem of synchronizing a network of semi-passive mobile sensors that compared to monolithic solutions involving large, specialized, and human operated surface vessels, teams of autonomous and minimally actuated mobile sensors can cover large expanses of physical space at reasonably low costs [1]. This can be accomplished by utilizing inexpensive sensing, computation, and communication hardware and increasing each vehicle's endurance by lowering onboard energy consumption [2]–[5]. Since energy expenditure due to mobility is significantly higher compared to sensing and communication, it makes sense to consider strategies where the drifters leverage the surrounding currents for their actuation needs [6], [7].

In this work, we consider scenarios where mobile sensors have limited communication range and thus must be within proximity of one another for data exchanges. (Although specifically targeted in this work which employs primarily surface vehicles, such cases are even more often in underwater robot deployments [8], [9].) In this context, the cooperative control strategy suggested rests on the assumption that mobile sensors can leverage the surrounding currents for navigation and controls is exerted to ensure they come into close proximity of one other, *i.e.*, rendezvous [10], to allow current and future data exchanges. The data can then be propagated throughout the network and fused accordingly.

We assume that the team of mobile networks operate in a region whose environmental dynamics can be reasonably approximated by gyre-like flows whose boundaries are delineated by Lagrangian coherent structures (LCS). As such, the active drifters can utilize these currents for mobility and maintain the desired motions for data gathering and rendezvous with neighboring drifters using minimal onboard actuation. From our previous work [11], [12], we examined conditions under which drifters in neighboring gyres can move into close proximity of one another by leveraging the flow dynamics in their respective gyre and achieve rendezvous, even in the presence of stochastic noise perturbing this dynamics [13]. An early synchronization control design that accompanied the derivation of periodic rendezvous conditions [11] treated the flow-induced drifter dynamics as harmonic oscillators and implemented a (linear) time-optimal control law aimed to synchronize the oscillators' phases, in an attempt to maximize the time they shared in the rendezvous region. While the periodic rendezvous conditions are valid in gyre flows [14], the *optimal* synchronization protocols needed to achieve rendezvous were not. Rather synchronization was achieved through the design of a sliding mode controller [14]. This paper presents a strategy that recovers time-optimality for the synchronization in gyre flows through a nonlinear transformation that brings the drifter dynamics into a form where a reasonable local approximation permits the application a time-optimal (bang-bang) synchronization controller. The efficacy and performance of this new time-optimal controller is validated via numerical and experimental studies.

Synchronization of coupled oscillators is an extensively studied field with applications in biology, physics, chemistry, among others [15]–[18]. Synchronization is achieved when the frequencies between neighboring harmonic oscillators agree [15]. The ability to synchronize is directly tied to the coupling strength between the oscillators [19] and thus when the oscillator dynamics is nonlinear, frequency synchronization does not necessarily guarantee phase matching.

Existing strategies in synchronization of coupled oscillators assume continuous and persistent interaction between the agents [20]. When the interaction is conditioned on proximity, synchronization must occur intermittently. Such intermittent interaction has not been well understood with the exception of [21]. In [21], Zavlanos coined such intermittent yet repeated rendezvous between robots as achieving *synchronous rendezvous* and developed strategies for ensuring

This work has been supported by ONR under grant #N000141712690.

Cong Wei and Bert Tanner are with the Department of Mechanical Engineering, University of Delaware, Newark DE 19716, USA; {weicong,btanner}@udel.edu .

Ani Hsieh are with the Department of Mechanical Engineering & Applied Mechanics, University of Pennsylvania, Philadelphia, PA 19104, USA; {m.hsieh}@seas.upenn.edu .

The authors thank Dhanushka Kularatne for his contributions in their experimental studies and Adam Stager for his help in designing the flow generator.

synchronous rendezvous at pre-specified sites for robots moving back and forth along the edges of a graph. By designing the mobile robot network to have a bipartite graph topology, the travel and wait times at rendezvous sites are set to ensure following synchronization.

Similar to [21], we assume robots can only interact intermittently, over very short time windows, and there is no information sharing nor control action when robots are outside their designated rendezvous neighborhoods. Different from [21], the motions of the robots and the topology of the resulting communication network is dictated by the underlying geophysical fluid dynamics where a bipartite graph structure may not be achievable. Furthermore, the active drifters may not have the necessary energy budget to achieve robust station-keeping given the ambient dynamics. Thus our approach leverages the surrounding environmental dynamics as vehicles attempt synchronous rendezvous.

Thus, this work reports on a control strategy that enables mobile sensors deployed in gyre flows to travel along adjacent limit cycles achieving periodic rendezvous such that they maximize the time they spend in the rendezvous zones (Section III). Through the proposed time-optimal controller, the underlying transformation applied to the nonlinear ambient flow improves on our previous strategy [14] by allowing for more realistic environmental dynamics. We present results from numerical studies designed to test the correctness of the control law for robots on a network of gyre flows (Section IV-A) and present experimental results to show the efficacy of the methodology in real physical environments (Section IV-B).

II. Problem statement

Denote (x_i, y_i) the position of drifter i with respect to some fixed Cartesian coordinate frame, and assume that the drifter moves under the influence of some double-gyre flow. For the double-gyre flow dynamics (Fig. 2) the amplitude and scale parameters are A and s, respectively [22]. When the agent is passively drifting without applying any actuation, its dynamics is

$$\dot{x}_i = -\pi A \ \sin \tfrac{\pi}{s} x_i \ \cos \tfrac{\pi}{s} y_i \tag{1a}$$

$$\dot{y}_i = \pi A \ \sin \tfrac{\pi}{s} y_i \ \cos \tfrac{\pi}{s} x_i \ . \tag{1b}$$

Now zoom out and imagine a planar array of gyres (Fig. 2), each indexed with the Cartesian coordinates (l, m) of its center. The area $D_{(l,m)}$ covered by gyre (l, m) is defined as the region

$$\Big\{x, y \in \mathbb{R}^2 \mid (x, y) \in [l - \tfrac{s}{2}, l + \tfrac{s}{2}] \times [m - \tfrac{s}{2}, m + \tfrac{s}{2}]\Big\} \ .$$

With C ranging in $[-1, 1]$, and with fixed (l, m), a gyre is characterized by a family $\Phi_{(l,m)}$ of invariant orbits each denoted

$$\Phi^C_{(l,m)} = \Big\{(x, y) \in D_{(l,m)} \mid \sin \tfrac{\pi x}{s} \ \sin \tfrac{\pi y}{s} = C\Big\}$$

in the sense that $\Phi_{(l,m)} = \bigcup_C \Phi^C_{(l,m)}$, and therefore the whole region $D_{(l,m)}$ is positively invariant.

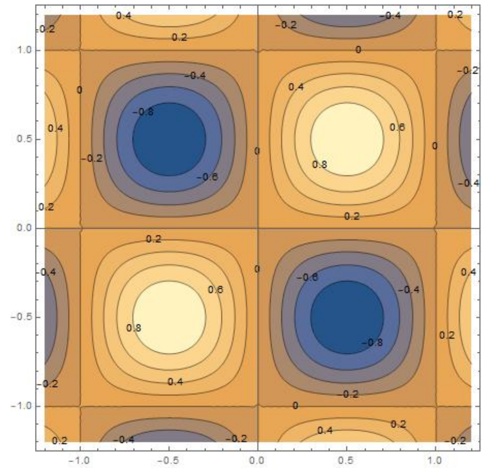

Fig. 1. Layout of the invariant orbits in the gyre lattice annotated by the values of parameter C.

We consider a lattice arrangement of gyres (see Fig. 1). Then with an appropriate selection of the global coordinate frame, the gyre centers take values $(^{Ms}/_2, {}^{Ns}/_2)$ for $M, \ N \in \mathbb{Z}$.

Definition 1 (Adjacent invariant orbits): Orbits $\Phi^{C_1}_{(l,m)}$ and $\Phi^{C_2}_{(r,q)}$ are *adjacent* if $C_2 = \pm C_1$ and

$$(r = l \pm s \wedge q = m) \ \vee \ (r = l \wedge q = s \pm m) \ .$$

For simplicity, we assume only one drifter drifting in each gyre, and we mark the symbolic coordinates of the gyre and that of the drifter with the same subscript i: agent i drifts in gyre (l_i, m_i). Drifters drifting along adjacent orbits are considered *neighbors*. Neighbors can only exchange information only when they are within distance δ of each other, and δ is called the *communication range*. When neighbors i and j satisfy $(x_i - x_j)^2 + (y_i - y_j)^2 \leq \delta^2$ then they are in *rendezvous*.

Definition 2 (Rendezvous): Neighbors i and j drifting along $\Phi^C_{(l_i,m_i)}$, $\Phi^{-C}_{(l_j,m_j)}$, respectively, are at *rendezvous* at time $\tau > 0$ if their Euclidean distance $d_{ij}(t)$ satisfies $d_{ij}(\tau) \leq \delta$.

Only when an agent is in rendezvous does it engage its controller. Then, the dynamics of agent i change from that of a passive drifter (1) to

$$\dot{x}_i = -\pi A \sin \frac{\pi}{s} x_i \cos \frac{\pi}{s} y_i + u_{x_i}(t - \tau) \tag{2a}$$

$$\dot{y}_i = \pi A \sin \frac{\pi}{s} y_i \cos \frac{\pi}{s} x_i + u_{y_i}(t - \tau) \tag{2b}$$

with u_{x_i} and u_{y_i} the control inputs along the corresponding spatial dimensions.

Spontaneous rendezvous, and consequently agent interaction, can be very ephemeral. Ideally, the rendezvous event is as frequent as possible and its duration is maximal — to safely allow e.g. complete data transmittal. For this to happen, cooperative control actuation has to be applied; however, the duration of this control intervention is limited within the time boundaries of the rendezvous event: drifters cannot interact when not in rendezvous. In other words, the controller needs to make the most of its (rendezvous) time to bring the adjacent drifters back together soon and allow them to stay together longer. This suggests a *time-optimal* control problem which is stated as follows:

Problem 1: Design a time-optimal cooperative control law which ensures that at steady state neighbors passively drifting according to (1) rendezvous as frequently as possible and stay in rendezvous for the maximum time (allowable by (2)).

III. Technical approach

Express the motion of the drifters in polar coordinates:

$$\theta_i = \operatorname{arctan2}(y_i - m_i, x_i - l_i) \tag{3a}$$
$$\rho_i = \|(x_i - l_i, y_i - m_i)\| \ . \tag{3b}$$

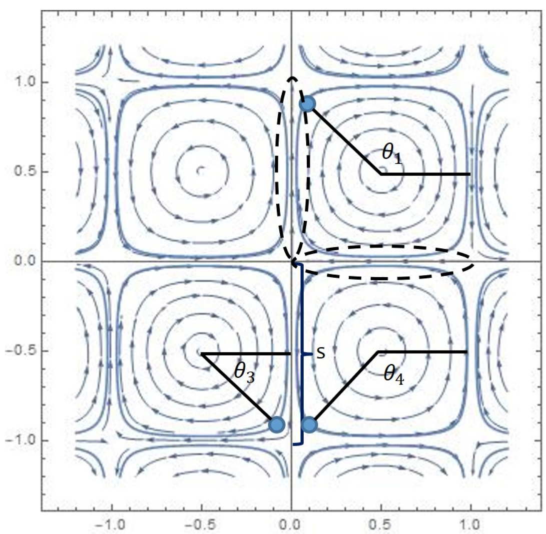

Fig. 2. Flow field of wind driven double gyre flow. One invariant orbit(bold contours) is with $|C| = 0.08$. The streamlines in oval circles are parts of hyperbolic manifolds. These three solid dots represent neighbor drifters which synchronize with each other.

Definition 3 (Pairwise synchronization): Two neighbors i and j, drifting along orbits $\Phi^{C}_{(l_i,m_i)}$ and $\Phi^{-C}_{(l_j,m_j)}$, respectively, achieve *pairwise synchronization* if

$$\theta_i + \theta_j = \begin{cases} 0 & \text{if } m_i = m_j \\ \pi & \text{otherwise} \end{cases} \tag{4a}$$
$$\rho_i - \rho_j = 0 \ . \tag{4b}$$

The condition for phase synchronization (4a) recognizes phase as a variable of interest (Fig. 2) and makes this approach easier to relate to existing literature. At the same time, tuning the radii to satisfy (4b) and synchronizing the phases according to (4a) is also in line with the definition of synchronization utilized in previous work [14].

A. Phase and radius dynamics for actuated drifter

The differential relation between the polar and Cartesian representations follows directly from differentiating (3)

$$\dot\theta_i = \tfrac{1}{\rho_i}(\dot y_i \cos\theta_i - \dot x_i \sin\theta_i)$$
$$\dot\rho_i = \dot x_i \cos\theta_i + \dot y_i \sin\theta_i \ .$$

If one uses (1) and (3) to substitute for the Cartesian variables and derivatives can be reduced to a form

$$\begin{aligned}\dot\theta_i &= f(\theta_i, \rho_i) \qquad\qquad (6a)\\ &\triangleq -\tfrac{\pi A}{\rho_i}\cos\theta_i \sin\left(\tfrac{\rho_i \pi}{s}\cos\theta_i\right)\cos\left(\tfrac{\rho_i\pi}{s}\sin\theta_i\right)\\ &\quad - \tfrac{\pi A}{\rho_i}\sin\theta_i \sin\left(\tfrac{\rho_i\pi}{s}\sin\theta_i\right)\cos\left(\tfrac{\rho_i\pi}{s}\cos\theta_i\right)\\ \dot\rho_i &= g(\theta_i,\rho_i) \qquad\qquad (6b)\\ &\triangleq \pi A \cos\theta_i \cos\left(\tfrac{\rho_i\pi}{s}\cos\theta_i\right)\sin\left(\tfrac{\rho_i\pi}{s}\sin\theta_i\right)\\ &\quad - \pi A \sin\theta_i \cos\left(\tfrac{\rho_i\pi}{s}\sin\theta_i\right)\sin\left(\tfrac{\rho_i\pi}{s}\cos\theta_i\right) \ ,\end{aligned}$$

which can be brought into a general form during rendezvous with cooperative control action being applied

$$\dot\theta_i = f(\theta_i,\rho_i) + u_{\theta_i}(t-\tau)$$
$$\dot\rho_i = g(\theta_i,\rho_i) + u_{\rho_i}(t-\tau) \ ,$$

where now the control inputs are understood along the radial and tangential (rate of rotation) dimensions. Note, however, that on a fixed orbit, θ and ρ are coupled:

$$\sin\left(\tfrac{\pi_i}{s}\rho_i\cos\theta_i + l_i\right)\sin\left(\tfrac{\pi}{s}\rho_i\sin\theta_i + m_i\right) = C \ .$$

The synchronization controller of the following section will therefore apply on the phases (6a) only.

B. Time optimal synchronization controller design

Define $\epsilon_{ij} \triangleq \theta_i + \theta_j$. Here we wrap $\epsilon_{ij} \in (-\pi, \pi]$. Given that the communication range is negligible compared to the scale of gyre, i.e, $\delta \ll s$, when two neighbors are in rendezvous

$$\epsilon_{ij}(\tau) \approx \begin{cases} 0 & \text{if } m_i = m_j \\ \pi & \text{otherwise} \end{cases}$$

and at the same time from (6) one can verify that

$$f(\theta_i,\rho_i) + f(\theta_j,\rho_j) \approx 0 \ .$$

Now define

$$u_{\theta_{ij}}(t) \triangleq u_{\theta_i}(t) + u_{\theta_j}(t) \tag{8}$$

in order to approximate the error dynamics in the form

$$\dot\epsilon_{ij} = u_{\theta_{ij}} \ . \tag{9}$$

Proposition 1: Consider a pair of neighbor drifters i and j for which $\theta_i + \theta_j$ is either in the neighborhood of 0 (or π), and their phase error dynamics is given by (9). Assume that the control input is bounded in the form $|u_{\theta_{ij}}(t)| \le \Delta \in \mathbb{R}_+$. Then the time-optimal control law $u_{\theta_{ij}}(t)$ to steer (9) to 0 (or π) is unique, given by

$$u^*_{\theta_{ij}}(t) = -\Delta \operatorname{sign}(\epsilon_{ij}) \ . \tag{10}$$

Proof: Optimizing for time, the Hamiltonian for (9) is

$$H = 1 + u_{\theta_{ij}}(t) p_1(t) \ ,$$

where the costate variable $p_1(t)$ satisfies

$$\dot{p}_1(t) = -\frac{\partial H}{\partial \epsilon_{ij}(t)} = 0 \ . \tag{11}$$

The control law $u_{\theta_{ij}}$ which minimizes the Hamiltonian is

$$u_{\theta_{ij}}(t) = -\Delta \operatorname{sign}\big(p_1(t)\big)$$

and assuming $p_1(0) = \pi_1$, it follows from (11) that

$$p_1(t) = \pi_1 = \text{constant} \ ,$$

at least piece-wise in time. With *constant* $u_{\theta_{ij}}(t) = \Omega \in \{-\Delta, 0, \Delta\}$, and initial condition $\epsilon_{ij}(0) = \xi_1$ (9) yields

$$\epsilon_{ij}(t) = \xi_1 + \Omega t \ .$$

Naturally, Ω has opposite sign from ξ_1 to reduce ϵ_{ij} and the switching point for Ω will be $\epsilon_{ij} = 0$, resulting to

$$u_{\theta_{ij}}(t) = \begin{cases} \Delta & \text{if } \epsilon_{ij} < 0 \\ 0 & \text{if } \epsilon_{ij} = 0 \\ -\Delta & \text{if } \epsilon_{ij} > 0 \ . \end{cases}$$

■

C. Control allocation

In view of (8), $u_{\theta_{ij}}$ can be realized in an infinite number of combinations of drifter i and j inputs. For instance, drifters can split the required control effort between them to balance the load on their onboard power resources. Another way could be to assign actuation loads according to individual energy reserves. This paper does not focus explicitly on the *optimal* control allocation problem; rather, it follows prior work [11] in which there is a leader-follower relationship between the drifters in rendezvous. A leader-follower relationship can suggest a control allocation strategy, especially in practical cases when it may be easier for the drifter to speed up along the current flow than fight against it. In such cases, the direction of actuation along u_{θ_i} and u_{θ_j} aligns with the current, which implies that the follower uses actuation to "catch up" and the control input of the follower satisfies

$$u_{\theta_k} \dot{\theta}_k \geq 0 \qquad k \in \{i, j\} \ . \tag{12}$$

Thus in this allocation strategy, the follower is responsible for optimizing rendezvous. (However, in a multi-pair network setting, this control load allocation strategy has its implications —details in Section IV-A.2.)

IV. Validation

A. Simulation

In all scenarios here, drifter oscillation frequencies here are fixed, determined by the ambient geophysical dynamics.

1) Synchronization for neighbor drifters: Two drifters on orbits $\Phi^{C}_{(\frac{s}{2},\frac{s}{2})}$ and $\Phi^{-C}_{(-\frac{s}{2},\frac{s}{2})}$ are released at initial positions $(0.7500, 0.0913)$ and $(-0.6500, 0.0721)$, respectively. The double-gyre flow dynamics parameters are set at $A = 0.03$, $s = 1$,and $C = 0.2$. The communication range is $\delta = 0.3$.

Based on these parameters, the period on the orbits $\Phi^{C}_{(\frac{s}{2},\frac{s}{2})}$ and $\Phi^{-C}_{(-\frac{s}{2},\frac{s}{2})}$ is 40.75 seconds. At 7.54 seconds after their release, the drifters come into rendezvous. During this first rendezvous, which lasts 10.47 seconds, control law (10) starts synchronizing the phases. Note that synchronization control action is only possible during rendezvous (marked by the time intervals of the red pulses in Figs. 3–4). As more clearly seen at the top graph of Fig. 3, during the first rendezvous (before the 20th second) the $\epsilon_{12} - \pi$ oscillation average drops, but does not yet vanish. During the subsequent period when the vehicles are no longer in rendezvous it remains constant (no control is applied), and then the synchronization controller zeros the error $\epsilon_{12} - \pi$ within the second rendezvous period. After synchronization is achieved, both $\epsilon_{12} - \pi$ and $\rho_1 - \rho_2$ remain at zero. Figure 4 depicts the evolution of the synchronization errors in Cartesian coordinates (cf. [14]).

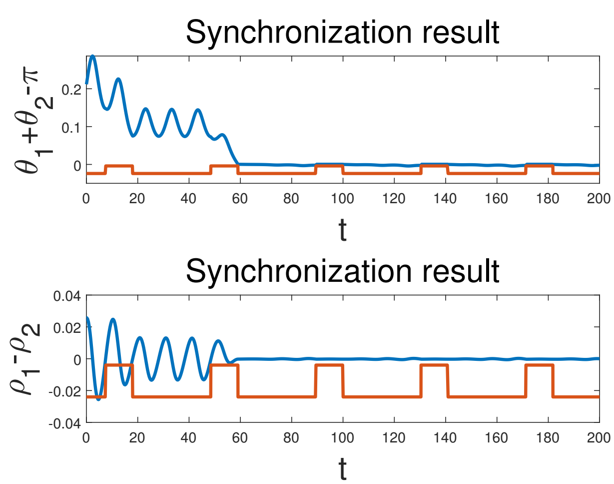

Fig. 3. Time evolution of $\theta_1 + \theta_2 - \pi$ and $\rho_1 - \rho_2$. The red square pulse train indicates when there is rendezvous.

2) Synchronization for a network of four drifters: Now four drifters are considered in a gyre configuration that matches that of Fig. 2. The drifters are indexed 1 through 4, and are deployed on orbits $\Phi^{0.1}_{(\frac{s}{2},\frac{s}{2})}$, $\Phi^{-0.1}_{(\frac{s}{2},\frac{3s}{2})}$, $\Phi^{0.1}_{(\frac{3s}{2},\frac{3s}{2})}$, and $\Phi^{-0.1}_{(\frac{3s}{2},\frac{s}{2})}$, respectively. The gyre flow parameters are set at $A = 0.03$, $s = 1$, and $C = 0.1$, while the communication range now is adjusted to $\delta = 0.4$. The initial positions for the four drifters are $(0.9681, 0.5000)$, $(0.9630, 1.3315)$, $(1.0741, 1.1427)$, and $(1.2384, 0.9573)$, respectively.

No drifter can rendezvous with all three others —only one at a time— so the interaction and communication topology is time-varying. If all four drifters are to be synchronized, they would need to converge to a state where (given the spatial

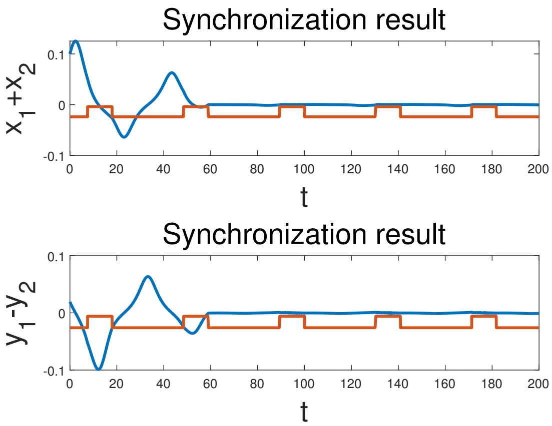

Fig. 4. Time evolution of $x_1 + x_2$ and $y_1 - y_2$. The red square pulse train indicates when there is rendezvous.

configuration of their gyres)

$$
\begin{aligned}
\epsilon_{12} &= \theta_1 + \theta_2 = \pi \ , & \rho_1 - \rho_2 &= 0 \\
\epsilon_{23} &= \theta_2 + \theta_3 = 0 \ , & \rho_2 - \rho_2 &= 0 \\
\epsilon_{34} &= \theta_3 + \theta_4 = \pi \ , & \rho_3 - \rho_4 &= 0 \\
\epsilon_{41} &= \theta_4 + \theta_1 = 0 \ , & \rho_4 - \rho_1 &= 0 \ .
\end{aligned}
$$

In this particular simulation example, drifter neighbor pair $(2, 3)$ rendezvous first, followed by $(1, 2)$, then $(1, 4)$ and finally $(3, 4)$. The history of the pairs' synchronization errors is shown in Fig. 5, and reveals an interesting consequence of the control allocation strategy of Section III-C.

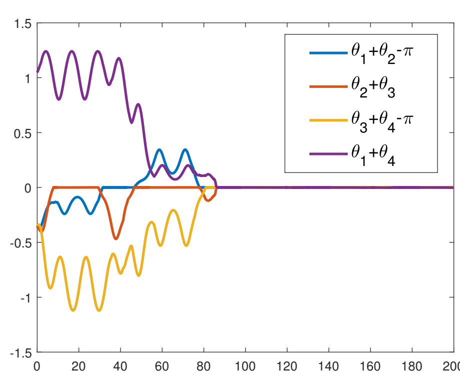

Fig. 5. Evolution of phases combination for the network.

When two drifters meet in isolation, they would activate their synchronization controllers and attempt to drive their synchronization errors to zero (see Fig. 3); if, however, a third drifter and engages with them while this synchronization is in process, this new control action under the control allocation scheme of Section III-C is bound to increase the synchronization errors related to the earlier rendezvous. For the whole network, synchronization error is updated for every period and vanishes at the end of the second period for the case in Fig. 3.

B. Experiment

Experiments were conducted in the multi-robot Coherent Structure Testbed (mCoSTe) at the University of Pennsylvania. The testbed consists of a $4.5\text{m} \times 3\text{m} \times 1.5\text{m}$ multi-robot flow tank (Fig. 6(b)) and a collection of micro autonomous surface vehicles (mASVs) (Fig. 6(a)). Each mASV is a differentially driven vehicle, with a maximum forward speed of 0.2m/s. As implied in Fig. 6(a), mASV localization is achieved through a motion capture system (see also [22] for details).

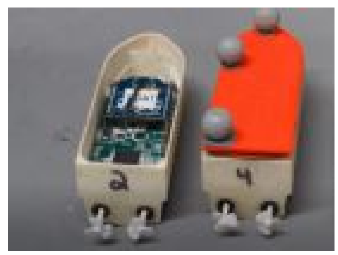

(a) micro Autonomous Surface Vehicle

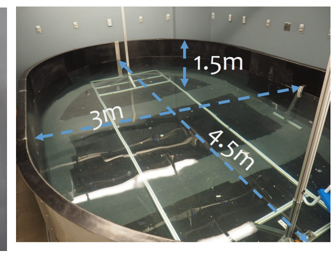

(b) Water tank and its sizes

(c) New flow generator

(d) Old flow generator

Fig. 6. Basic setup for water tank experiment. Source: ScalAR Lab

The current circulation within the flow tank is generated by motor actuators, that feature newly designed 3D printed propellers. Compared to earlier gyre flow realizations (Fig. 6(d)) [22], the new flow generator system (Fig. 6(c)) can create a steady desired current flow faster and requires less maintenance. Custom propeller blades had to be designed and manufactured in order to produce the opposite flow directions necessary to emulate a double-gyre flow.

To generate a combination of gyre flows, each pair of flow generators needs to utilize propellers with opposite directions of rotation. The pair of propellers utilized in Fig. 8 is placed at a distance of 1m along the x axis and symmetrically with respect to the y axis. The propeller rotation speed is 70 rpm. The streamlines produced resemble the hyperbolic manifold associated with (1). To keep the robotic mASVs along their Φ^C orbits, a PID tracking controller is employed, steering each robot to track a reference point that evolves according to (1). The outcome of this tracking controller is shown in Fig. 7 for the two mASVs participating in this experiment.

Tho mASVs are initially placed at coordinates $(0.6779, 1.8726)$ and $(-0.8326, 1.6792)$. Their orbits are identified as $\Phi^{-0.2}_{(0.5,1.5)}$ and $\Phi^{0.2}_{(-0.5,1.5)}$, and the amplitude and scale parameters of the experimentally produced field are approximated at $A = 0.03$, and $s = 1$, respectively,

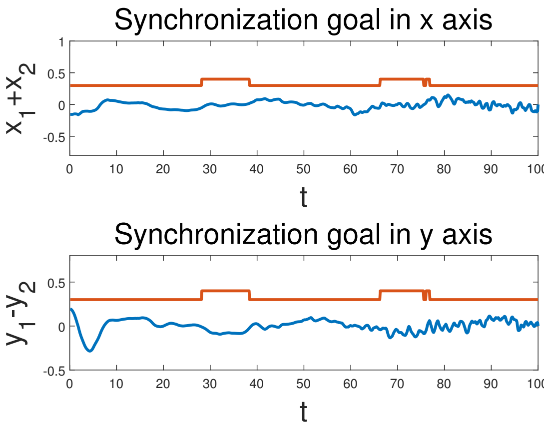

Fig. 9. Evolution of $x_1 + x_2$ and $y_1 - y_2$. The red square pulse train marks the rendezvous periods.

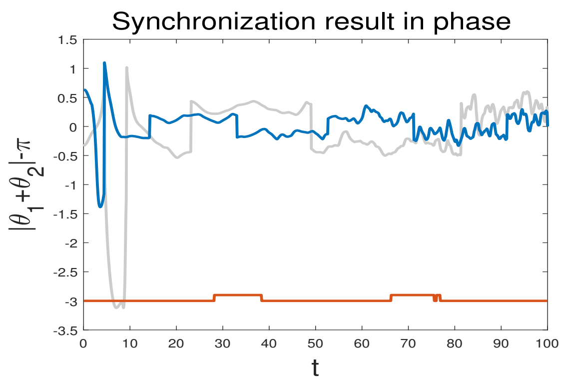

Fig. 10. Evolution of $|\theta_1+\theta_2|-\pi$ during the experiment. The red piecewise constant line indicates the periods of rendezvous. The blue curve shows the history of the phase error ϵ_{12}. The gray curve shows the error evolution in another baseline experiment where the synchronization controller was not active, for comparison purposes.

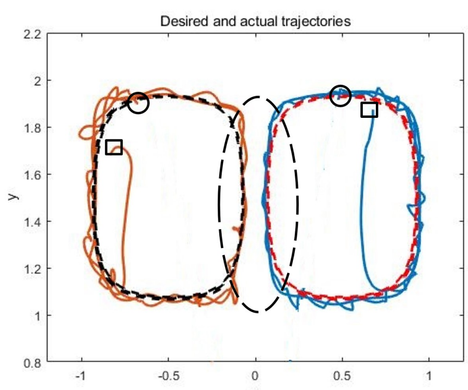

Fig. 7. The effect of the PID tracking controller: Reference orbits (dashed curves) and actual vehicle trajectories (colored curves). Initial positions are marked by squares and the circles show the vehicle positions at the end of the experiment. The dashed oval highlights the portion of the orbits where rendezvous occurs.

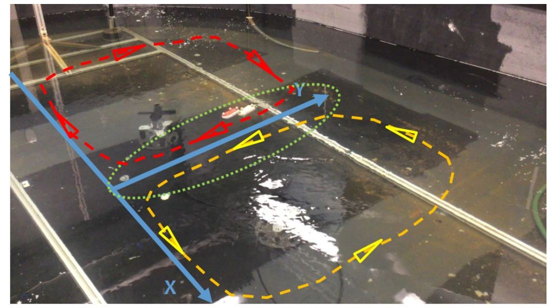

Fig. 8. An image snapshot during the experiment. The yellow and red paths mark the desired (theoretical) orbits for two mASVs.

while the communication (rendezvous) range is $\delta = 0.3$.

This experiment runs for 100 seconds. After 28.2 seconds since being released, the two mASVs have their first rendezvous (see Fig. 9). The time optimal control law engages and for the brief 10.1 second time window of this encounter, one vehicle regulates its speed relative to the other. The second rendezvous begins at 66.3 seconds and lasts for 10.5 seconds —0.4 seconds longer than the first one. The evolution of the synchronization errors in Cartesian coordinates, $x_1 + x_2$ and $y_1 - y_2$, are shown in Fig. 9. The evolution of the synchronization errors in phases, $|\theta_1 + \theta_2| - \pi$ is shown in Fig. 10. The effect of (random, for the most part) environmental disturbances is evidence in the measurements, but the controller keeps the errors bounded at a lower level compared to when control action is not applied.

V. Conclusion

Mobile sensors drifting along ocean circulations can leverage ambient environmental dynamics to navigate, search, and monitor dynamic marine environment and minimize energy expenditure. In situations where robots are limited to short-range communication while deployed over large swaths of ocean, they must take advantage of times when the ocean dynamics bring them within proximity of each other to interact. This robot-environment interaction can improve the efficiency of the sensor network for data uploads, exchanges, backups, and such. Therefore it makes sense for these robots to maximize their time for regularity of interaction. This can be possible through cooperative, intermittent time-optimal control policies which take into account the nonlinear dynamics —at least in idealized form— of the ocean circulation currents that drive the gross, large-scale motion of those robots. This idea is explored and tested in a novel small-scale experimental testbed where circulation is generated artificially through a system of submerged propeller-based flow generators. The time-optimal cooperative control law reported here is an example of a local robot interaction policy that works in concert with strong ambient environmental dynamics to yield emergent network properties. More work is needed to understand how the allocation of the cooperative control action between the robots in rendezvous can affect the global synchronization abilities of a network of robotic drifters flowing along neighboring gyre flows.

References

[1] E. A. D'Asaro, "Performance of autonomous Lagrangian floats," *Journal of Atmospheric and Oceanic Technology*, vol. 20, no. 6, pp. 896–911, 2003.

[2] A. Molchanov, A. Breitenmoser, S. Subbaraya, and G. Sukhatme, "Active Drifters : Sailing with the Ocean Currents," in *RSS Workshop on Autonomous Control, Adaptation, and Learning for Underwater Vehicles*, 2014.

[3] A. Valada, P. Velagapudi, B. Kannan, C. Tomaszewski, G. Kantor, and P. Scerri, *Development of a low cost multi-robot autonomous marine surface platform*, vol. 92. Springer, Berlin, Heidelberg, 2014.

[4] Z. Song, D. Lipinski, and K. Mohseni, "Multi-vehicle cooperation and nearly fuel-optimal flock guidance in strong background flows," *Ocean Engineering*, vol. 141, pp. 388–404, 2017.

[5] J. Moulton, N. Karapetyan, M. Kalaitzakis, A. Q. Li, N. Vitzilaios, and I. Rekleitis, "Dynamic Autonomous Surface Vehicle Controls Under Changing Environmental Forces," *arXiv preprint arXiv:1908.02850*, 2019.

[6] J. Hansen, S. Manjanna, A. Q. Li, I. Rekleitis, and G. Dudek, "Autonomous Marine Sampling Enhanced by Strategically Deployed Drifters in Marine Flow Fields," in *MTS/IEEE OCEANS*, pp. 1–7, 2018.

[7] J. Jouffroy and O. Zielinski, "On Active Current Selection for Lagrangian Profilers," *Identification and Control*, vol. 34, no. 1, pp. 1–10, 2013.

[8] J. Das, F. Py, T. Maughan, T. O'Reilly, M. Messié, J. Ryan, G. S. Sukhatme, and K. Rajan, "Coordinated sampling of dynamic oceanographic features with underwater vehicles and drifters," in *International Journal of Robotics Research*, vol. 31, pp. 626–646, SAGE, London, UK, apr 2012.

[9] V. Yordanova and H. Griffiths, "Synchronous rendezvous technique for multi-vehicle mine countermeasure operations," in *MTS/IEEE OCEANS*, pp. 1–6, 2015.

[10] N. Roy and G. Dudek, "Collaborative robot exploration and rendezvous: Algorithms, performance bounds and observations," *Autonomous Robots*, vol. 11, pp. 117–136, sep 2001.

[11] C. Wei, C. Li, and H. G. Tanner, "Synchronous Rendezvous for Periodically Orbiting Vehicles with Very-Low-Range Interactions," in *Proceedings of the IEEE American Control Conference*, pp. 1641–1646, 2018.

[12] C. Wei, X. Yu, H. G. Tanner, and M. A. Hsieh, "Synchronous rendezvous for networks of active drifters in gyre flows," in *Distributed Autonomous Robotic Systems* (N. Correll, M. Schwager, and M. Otte, eds.), (Cham), pp. 413–425, Springer International Publishing, 2019.

[13] X. Yu, M. A. Hsieh, C. Wei, and H. G. Tanner, "Synchronous Rendezvous for Networks of Marine Robots in Large Scale Ocean Monitoring," *Frontiers in Robotics and AI*, vol. 6, p. 76, sep 2019.

[14] C. Wei, H. G. Tanner, X. Yu, and M. A. Hsieh, "Low-Range Interaction Periodic Rendezvous Along Lagrangian Coherent Structures," in *Proceedings of the IEEE American Control Conference*, pp. 4012–4017, July 2019.

[15] A. Pikovsky, M. Rosenblum, J. Kurths, and R. C. Hilborn, "Synchronization: A Universal Concept in Nonlinear Science," *American Journal of Physics*, vol. 70, no. 6, pp. 655–655, 2002.

[16] E. M. Izhikevich, *Dynamical systems in neuroscience : the geometry of excitability and bursting*. MIT Press, 2007.

[17] J. Cortés, "Oscillations and Coupling in Interconnections of Two-Dimensional Brain Networks," in *Proceedings of the IEEE American Control Conference*, pp. 193–198, 2019.

[18] M. Tyloo and P. Jacquod, "Global Robustness vs. Local Vulnerabilities in Complex Synchronous Networks," *arXiv preprint arXiv:1905.03582*, pp. 1–11, 2019.

[19] A. Jadbabaie, N. Motee, and M. Barahona, "On the Stability of the Kuramoto Model of Coupled Nonlinear Oscillators," in *Proceedings of the IEEE American Control Conference*, pp. 4296–4301, 2004.

[20] J. Alonso-Mora, E. Montijano, T. Nägeli, O. Hilliges, M. Schwager, and D. Rus, "Distributed multi-robot formation control in dynamic environments," *Autonomous Robots*, vol. 43, no. 5, pp. 1079–1100, 2019.

[21] M. M. Zavlanos, "Synchronous rendezvous of very-low-range wireless agents," in *Proceedings of the IEEE Conference on Decision and Control*, pp. 4740–4745, 2010.

[22] D. Kularatne, S. Bhattacharya, and M. Ani Hsieh, "Time and Energy Optimal Path Planning in General Flows," in *Robotics: Science and Systems XII*, Robotics: Science and Systems Foundation, 2016.